CHAPTER I

CONVERSION OF BIOPITCH TO CARBON FOAM WITH TUNABLE PROPERTIES: THE ROLE OF CHEMICAL ACTIVATION

Adife Seyda Yargic

(Asst. Prof. Dr.), Bilecik Şeyh Edebali University, Bilecik, Turkey
e-mail: seyda.guler@bilecik.edu.tr
0000-0002-8671-5896

1. Introduction

Carbon foams are cellular structures with characteristic sizes between 100-500 μm and involving randomly distributed pores. The properties of carbon foams can be listed as adjustable thermal and electrical conductivity, lightness, low thermal expansion, high thermal shock resistance, and mechanical strength (Gao, et al., 2018; Liu, et al., 2014; Wang, et al., 2016). These unique properties, which are primarily related to the features of the precursors and working parameters, turn carbon foams into high-performance engineering materials and become attractive for numerous application fields in industries (Tzvetkov, et al., 2016). Carbon foams are evaluated in various usages such as heat exchanger, high-temperature heat insulation, electromagnetic shielding, the electrode for fuel cells, catalyst support, sound/radar absorption, and filter (Antunes and Velasco, 2014; Elgafy and Mishra, 2014; Liu, et al., 2014; Lv, et al., 2012; Micheli, et al., 2014; Velasco, et al., 2010). Traditionally, carbon foams are produced by foaming pitch-based or organic polymer resins, curing in an inert atmosphere and applying carbonization/graphitization processes. Pitch-based carbon foams are in tendency to give a regular graphitic structure and reveal high thermal/electrical conductivities. On the contrary, carbon foams with amorphous structures are synthesized from synthetic polymer resins or naturally renewable materials (Chithra, et al., 2020).

In this study, carbon foam with adjustable properties was synthesized from the pistachio shell, which was renewable household waste, following the stages of pyrolysis, pitch production, foaming, and carbonization, respectively. Within the scope of examining the effect of the chemical activation process on carbon foam properties, it was aimed to increase porosity by applying activation with potassium hydroxide after the foaming process. In the last stage, comprehensive characterization

studies were carried out to determine the CHN content by elemental analysis of carbon foams, to examine their structural, morphological, and crystallographic properties, and to calculate porosity and compression strength values to get information about structure-property relevance.

2. Materials and Methods

2.1. The Characteristics of Waste Biomass

Pistachio shells (*PS*) were first washed with distilled water and were left to dry under laboratory air. Then, the particle size of the raw material was minimized by operating Armfield FT-7A brand grinder and the mean particle size was estimated as 1.57 mm via particle size analysis. *PS* with a particle size in the range of 0.425> Dp> 0.25 mm was used in the experiments. The structural analyzes that determine the amounts of holocellulose, hemicellulose, extractive material, lignin, and cellulose, and also a preliminary analysis of the raw material including moisture, ash, volatile matter, and fixed carbon contents were performed based on ASTM standard test methods (Ozbay and Yargic, 2019). The ultimate analysis was carried out by examining the carbon, hydrogen, and nitrogen contents in the structure of *PS* with the organic sample burning process carried out in the elemental analysis device (Leco CNH628 S628) at 950 °C. The oxygen content was ascertained by subtracting the total amount of CHN% by weight obtained from the elemental analysis process from 100. Besides, thermal degradation behavior of *PS* with thermogravimetric analysis (TGA, Setaram Labsys Evo) and surface morphology with scanning electron microscopy (SEM, Zeiss Supra VP 40) were investigated, and functional groups were recognized by Fourier transform infrared spectroscopy (FT-IR, Perkin Elmer Spectrum 100). Before SEM analysis, the material was platinum-coated under vacuum in the Quorum Q 150 R ES DC Sputter device. FT-IR spectra were taken using the attenuated total reflectance (ATR) technique with a spectral resolution of 4 cm^{-1} in the 4000-400 cm^{-1} scan range.

2.2. Pyrolysis of *PS* and Tar Production

Pyrolysis process was practiced in stainless steel (# 316) Heinze reactor under static atmospheric conditions at a heating rate of 7 °C/min. The temperature of the reactor was measured with a thermocouple and the heating of the system with the resistance furnace around the reactor was carried out in a controlled manner. The temperature of *PS* (15 g) was raised from T_{room} to the final pyrolysis temperature of 400 °C and it was held at this temperature for 20 minutes until no remarkable gas evolution was observed. After condensing the tar and aqueous phase mixture in liquid collection traps at 0 °C, they were washed with dichloromethane and the tar was transferred into the organic phase by splitting up in the separation funnel. In the last stage, the aqueous phase that may have passed into the

organic phase was caught by using anhydrous sodium sulfate, and then the tar yield was calculated by separating the tar and solvent in the rotary evaporator. The solid product yield was determined by weighing the remaining part in the reactor, and the gaseous product yield was attained from the total mass balance. While determining the pyrolysis product distribution, calculations were made on a dry and ash-free basis (daf) and the mean of three runs was taken. Elemental analysis was accomplished to examine the structure of tar ($PS_{@400\ °C}$) to be used in the production of biopitch, FT-IR spectroscopy, proton nuclear magnetic resonance spectroscopy (^{1}H-NMR, Varian Mercury 300 MHz), and gas chromatography-mass spectroscopy (GC-MS, GC-2010 Plus) analysis methods were applied. In the GC-MS device, a TRB-5MS model column with dimensions of 30mx0.25mmx0.25μm was used and the peaks were identified using the Wiley7 library.

2.3. Biopitch Production Process from Tar

The biopitch to be used as a precursor in the fabrication of carbon foam was prepared from the heavy phase aromatic structures in the tar structure by the vacuum distillation process performed for 24 hours at 250 °C and 50 mbar vacuum pressure. The oxygen content in the structure of biomass-based tar causes the deterioration of the pitch structure at higher temperatures and the formation of solid thermofix carbon residue (Rocha, et al., 2002). Prauchner et al. (2004) found that during the formation of eucalyptus tar pitches through the distillation process at 250 °C, the C–O bonds in the structure were broken, and although the side chains were released, the heavier fractions in the aromatic ring reacted to create larger molecules. While highlighting the structure of the biopitch, ash content and softening point were determined, elemental analysis, helium gas pycnometer, thermogravimetric analysis, and Fourier transform infrared spectroscopy methods were applied.

2.4. Foaming, Carbonization and Activation Processes, Product Characterization

An inert atmosphere was provided with nitrogen gas during the foaming process of the biopitch performed in the Parr 4575B model reactor (Parr Instrument Company, USA). Synthesized-green foam, which was a semi-finished product, was produced by the process of heating the biopitch up to 450 °C with a heating rate of 2.5 °C/min at 1MPa reactor pressure and releasing the pressure after standing 1 hour at this temperature. To promote the surface area of the synthesized-green foam, a chemical activation process was applied with potassium hydroxide (KOH) in a ratio of foam: activation agent of 1:1 (Tondi, et al., 2010). The chemical reactions during the heat treatment applied to improve the surface area with the help of potassium hydroxide were detailed in the previous study

(Yargic and Ozbay, 2019). In the last stage, the synthesized-green foam and activated foam were heated to 1050 °C with a heating rate of 5 °C/min under a N_2 atmosphere (flow rate 100 mL/min) and carbonized for 2 hours in a tube furnace. The carbonized foams were coded as *PSCF* or *PSACF*, respectively, depending on whether they were synthesized or activated from the pistachio shell-based biopitch.

Elemental analysis, x-ray diffraction (XRD, PANalytical Empyrean, 2θ=0–80° range), scanning electron microscope (Zeiss Supra VP 40), nitrogen sorption (Micromeritics ASAP 2020, @ 77 K) techniques were used to analyze the characteristic properties of carbon and activated foams. Also, Shimadzu AG-IC 100KN with a loading speed of 0.5 mm/min was utilized to measure the compressive strengths. Finally, the bulk density of the foams was computed and the porosity(%) was calculated by measuring the actual density values with a helium pycnometer (Micromeritics, Accupyc II 1340).

3. Results and Discussion

3.1. The Properties of *PS*

The results of the ultimate and proximate analyses of the pistachio shell were presented in Table 1. According to the elemental analysis results, the higher heating value (HHV) of *PS* was calculated as 15.11 MJ/kg from the Dulong formula (Harker & Backhurst, 1981). The high volatile matter (80.68%) and low ash (2.12%) amounts of the PS with the carbon (47.10%) and lignin contents (27.36%) indicated that the selected biomass was suitable for the pyrolysis and biopitch preparation processes to be applied in the development of carbon foam. As shown in Figure 1, it was determined that *PS* consisted of particles with similar structures and had a non-porous morphology due to the image taken at 5000x magnification using the scanning electron microscope.

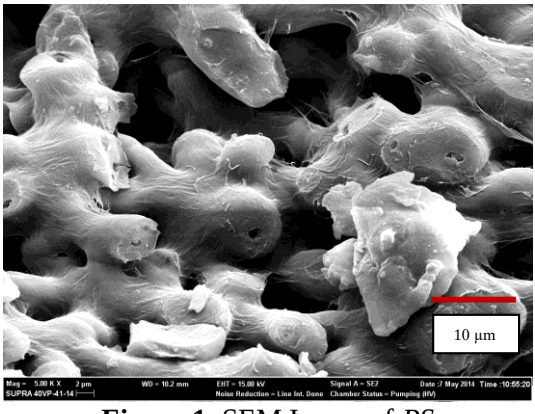

Figure 1. SEM Image of *PS*

Table 1. The Results of Ultimate and Proximate Analyses

Ultimate Analysis		
	PS	***PS*$_{@400\ °C}$**
Component (%)		
C	47.10	51.66
N	2.46	4.66
H	5.08	6.01
O[a]	46.70	37.67
Empirical formula	$CH_{1.29}N_{0.05}O_{0.75}$	$CH_{1.40}N_{0.08}O_{0.55}$
H/C	1.29	1.40
O/C	0.75	0.55
HHV (MJ/kg)	15.11	19.35
Proximate Analysis of PS		
Preliminary analysis	***wt.%.***	
Moisture	2.05	
Ash	2.12	
Volatiles	80.68	
Fixed Carbon[a]	15.15	
Structural analysis	***wt.%***	
Holocellulose	69.84	
Hemicellulose	23.05	
Extractives	0.68	
Lignin	27.36	
Cellulose[a]	46.79	
Average bulk density (g/cm^3)	0.71	

[a] Calculated by the difference.

TG and dTG curves of the thermogravimetric analysis applied to determine the thermal and pyrolytic behavior of *PS* were shown in Figure 2.a. According to the thermogravimetric analysis results, the moisture in the structure of *PS* was removed in the first step between 80 and 120 °C, the high weight loss was arisen due to the breakdown of cellulose and

hemicellulose through the pyrolysis reaction in the range of 180-450 °C, and the degradation process was slower between 450 and 550 °C with regards to the degradation of lignin (Yargıç et al., 2021). The ash and non-degradable C amounts in the structure of raw material were detected from the residue remaining from the thermogravimetric analysis.

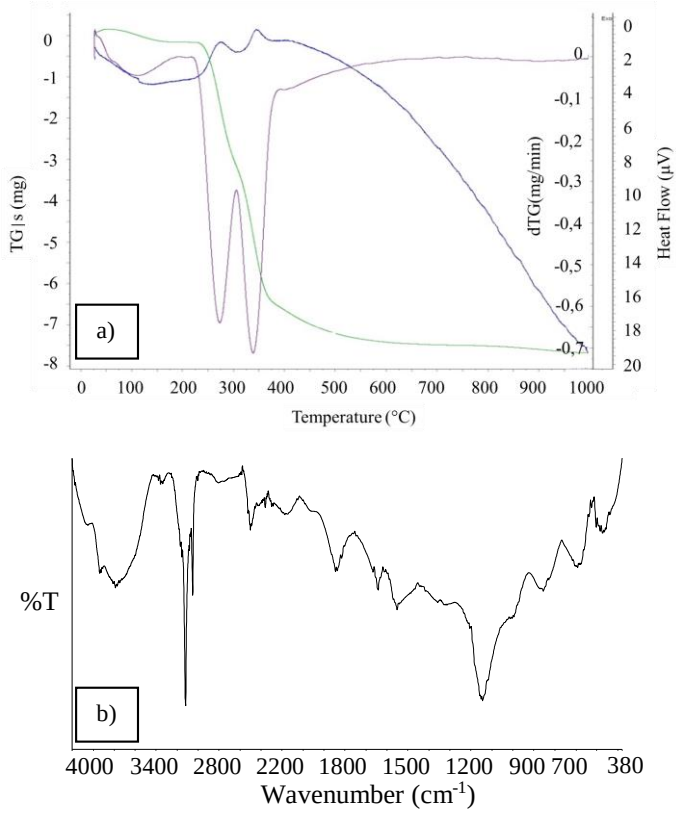

Figure 2. a) TG/dTG Curves and b) FT-IR Spectrum of *PS*

Due to the FT-IR spectrum taken to examine the functional groups in the PS structure (Figure 2b), the wide –OH band designating the presence of alcohol/phenol or carboxylic acids around 3600-3300 cm^{-1} (Apaydın-Varol and Erülken, 2015) and peaks indicating the entity of aliphatic structures and asymmetrical/symmetrical C–H vibrations between 2950-2800 cm^{-1} were determined. Strong peaks around 1770-1500 cm^{-1} referring to the existence of either ester, ketone, carboxylic acid, or aldehyde indicated the C=C stretching vibrations in aromatic and olefinic structures and C=O vibrations of the carbonyl group. Peaks in the band range of 1480-1420 cm^{-1}, which were an indicator of the presence of unsaturated ethers and phenols, defined C–H bending vibrations in aliphatic structures, and peaks between 1430-1200 cm^{-1} defined –CH bending vibrations of aliphatic methyl and methylene, and also C–O–C

stretching vibrations of unsaturated ethers. Finally, the C–O stretching band of lignin in the structure of biomass was detected with severe peaks around 1060-1020 cm^{-1}. Finally, the C–O stretching band of lignin in the structure of biomass was attributed to severe peaks around 1060-1020 cm^{-1} (Sun and Webley, 2011).

3.2. Pyrolysis Product Distribution and Characterization of Tar

According to the product distribution of the pyrolysis of *PS* at 400 °C, the gaseous and solid product yields were determined as 23.11% and 31.75%, respectively. Besides, tar and aqueous phase yields were calculated as 19.40% and 25.74%. As given in Table 1, the C content was detected as 51.66% and the higher heating value was 19.35 MJ/kg in reference to the elemental analysis of tar ($PS_{@400\ °C}$). Tar produced by thermal degradation of lignocellulosic biomass, which had a complex chemical structure, was found to be comprised of various organic compounds arising from the decomposition of cellulose, hemicellulose, and lignin. Functional groups specified to be in the structure of $PS_{@400\ °C}$ via FT-IR analysis and the atomic structures/groups to which these functional groups belong were presented in Table 2 related to their wavenumber values.

GC-MS chromatogram of $PS_{@400\ °C}$ tar and qualitative composition data of organic fractions defined according to GC-MS analysis results were given in Figure 3 and Figure 4, respectively. Chemical compounds were categorized related to GC-MS chromatogram as acids (AC), alcohols (AL), aldehydes (ALD), esters (EST), phenols (PH), ketones (KET), oxygenated aromatics (OxyAR), and oxygenated phenols (OxyPH). Among these compounds, phenols and aromatic hydrocarbons were classified as high value-added chemicals that could be utilized in the production of next-generation technological materials such as carbon foam or used as fuel (Yaman, et al., 2018). It was found that furan and vanillin compounds were formed in the tar due to the degradation of lignin, which was 27.36% in the pistachio shell with lignocellulosic structure, during the pyrolysis process. Furfural; 2-furan methanol; 2-methoxyphenol; 2-methoxy-4-methylphenol and 2,6-dimethoxyphenol compounds were found more in the composition of $PS_{@400\ °C}$ tar compared to other compounds.

Table 2. FT-IR Results and Functional Groups of $PS_{@400\ °C}$

Wavenumber (1/cm)	**Functional Groups**	**Atomic Structure and Groups**	***PS*** **@400 °C**
3600-3300	O–H stretching band	Hydroxyl, acid, phenol	3407
3040-3000	C–H stretching band	Aromatic ring	2995
2950-2800	C–H stretching band	Asymmetric and symmetric aliphatic CH_3 and CH_2	2938
1770-1650	C=O stretching band	Carbonyl group	1711
1625-1590	C=C stretching band	Olefinic structures	1625
1600,1580,1450	C=C stretching band	Aromatic structures	1515
1450 and 1375	C–H bending band	Aliphatic CH_3	1435 1364
1465	C–H bending band	Aliphatic CH_2	1463
1275-1200	C–O–C stretching band	Unsaturated ethers	1214
1200-1000	C–H out-of-plane bending band	Aromatic structures	1105
1060-1020	C–O–C stretching band	Aliphatic ether/ Primary or secondary alcohol	1020
900-700		Substituents on the aromatic ring	929, 883, 812, 755

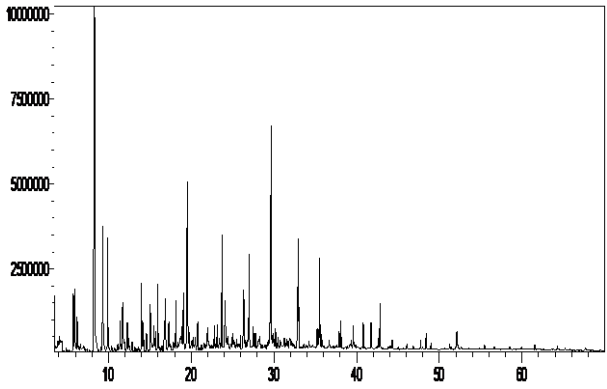

Figure 3. GC-MS Chromatogram of $PS_{@400\,°C}$

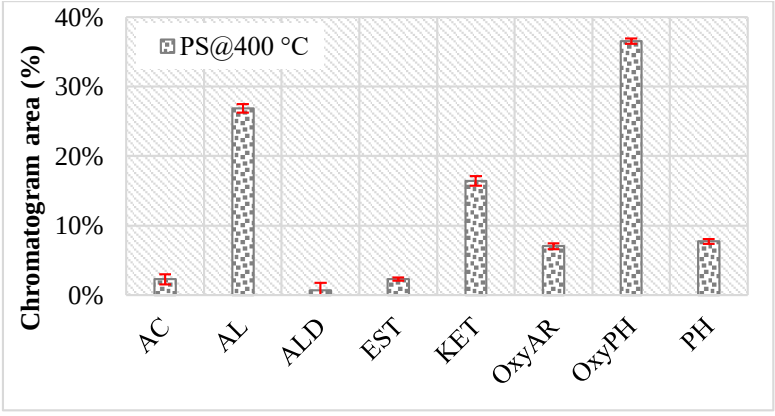

Figure 4. Chemical Composition of the Organic Fraction $PS_{@400\,°C}$

The results of the ^{1}H-NMR analysis applied to illustrate the hydrogen species in the structure of $PS_{@400\,°C}$ were represented in Table 3. According to the ^{1}H-NMR spectrum related to the chemical shift of the proton species, it was noticed that the proportion of hydrogen bonds in aromatic and phenolic compounds, which were noteworthy in biopitch and carbon foam formation, was high. Thus, it was concluded that;

i) Aromatic hydrogen bonds belonging to aromatics and conjugated olefins were found as 28.37% in the range of 9.0-6.0 ppm,

ii) Allylic and vinylic hydrogen bonds defining phenols and unconjugated olefins were ascertained as 8.04% in the range of 6.0-4.0 ppm.

Table 3. ^{1}H-NMR Analysis Results of $PS_{@400\ °C}$

Chemical shift range, δ (ppm)	**Hydrogen type**	***PS*$_{@400\ °C}$**
0.5-1.0	CH_3 and paraffinic CH_3 groups in γ or farther positions attached to the aromatic ring	2.31
1.0-1.5	CH_3, CH_2, and CH in the β position of the aromatic ring	8.66
1.5-2.0	CH_2 and CH attached to naphthenes	5.21
2.0-3.0	CH_3, CH_2, and CH in the α position of the aromatic ring	32.96
0.5-3.0	***TOTAL ALIPHATICS***	***49.15***
3.0-4.0	Hydroxyls, ring-binding methylene, methyl and methoxy	13.13
4.0-6.0	Phenols, non-conjugated olefins	8.04
6.0-9.0	Aromatics, conjugated olefins	28.37
9.0-12.0	Aldehydes and/or carboxylic acids	1.31

3.3. The Properties of Biopitch

The elemental analysis, softening point (SP) and actual density measurements, % ash and% yield calculation results of biopitch (*PS-P50-250°C-24h*) prepared from $PS_{@400\ °C}$ were given in Table 4. Accordingly, as a result of the vacuum distillation process carried out for 24 hours at 250 °C and 50 mbar vacuum pressure, the biopitch with a C content of 73.785% was produced with a yield of 20.37%. Considering the C content of the raw material (47.10%), it was stated that the C content of the biopitch was ~57% higher than the raw material. Besides, the ash amount of the biopitch structure was at a negligible level of 0.181% while the ash content in the *PS* structure was 2.12%. The softening point of *PS-P50-250°C-24h* was compatible with the softening points of biomass-based pitches in the literature and was measured as 129.8 °C (Prauchner, et al., 2004; Yargic and Ozbay, 2019).

Table 4. Biopitch Properties (T=250 °C, P=50mbar, t=24 h)

Precursor	***PS biopitch***
C (%)	73.785
H (%)	6.627
O (%)	18.695
N (%)	0.893
Pitch yield (%)	20.37
Ash (%)	0.181
Density (g/cm^3)	1.22
SP (°C)	129.8

The functional groups in the biopitch structure, which had a complex composition and contained lignin-derived compounds, were elucidated by examining the FT-IR spectrum (Figure 5). In reference to the FT-IR spectrum, peaks of –OH and –COOH for free alcohol and phenolic compounds near 3300 cm^{-1}, and CH stretching vibrations related to alkane structure around 2900 cm^{-1} were detected. The existence of C≡CH alkyne stretching vibrations was proved by the peak observed in the 2100 cm^{-1} band. Unconjugated C=O (aldehyde, ketone, carboxylic acid) stretching vibration peaks around 1700 cm^{-1}, C=C$_{ar}$ stretching band indicating the presence of aromatic structures between 1600 and 1400 cm^{-1}, CH bending band of guaiacyl- and syringyl- derivatives at 1115 cm^{-1} and finally, the peak of C=C cis bending band close by 750 cm^{-1} were observed (Araújo and Pasa, 2003; Araújo and Pasa, 2004; Melo and Pasa, 2003). The presence of hydroxyl and carboxyl groups referring to the existence of oxygenated derivatives such as alcohol, phenol, aldehyde, ketone, and carboxylic acid in the structure of the biopitch, which was determined to have 18.695% O content from the elemental analysis results, was supported by the FT-IR spectrum.

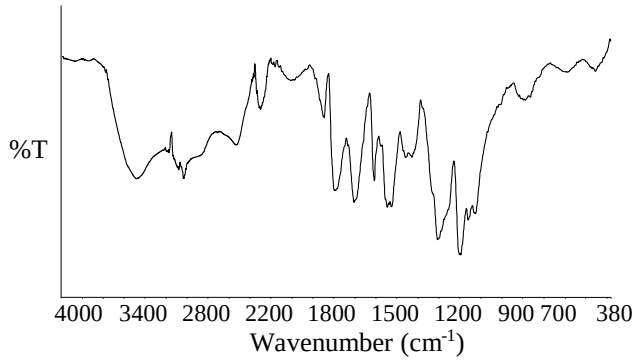

Figure 5. FT-IR Spectrum of *PS-P50-250°C-24h*

TG and dTG curves of the thermogravimetric analysis process performed by heating the biopitch under a nitrogen sweeping environment from room temperature to 1000 °C were shown in Figure 6. Regarding the TG curve, a residue (44%) was formed as a result of decomposition reactions that started at 200 °C and proceeded continuously up to 620 °C. The behavior of the biopitch against the heating process applied during the foaming process in the reactor was analyzed by the thermogravimetric analysis. Oxygen, which was ascertained to be ~ 19% via elemental analysis, moved away from the complex biopitch structure rich in aromatic components during the foaming process and caused 56% degradation of the biopitch as it supported self-combustion.

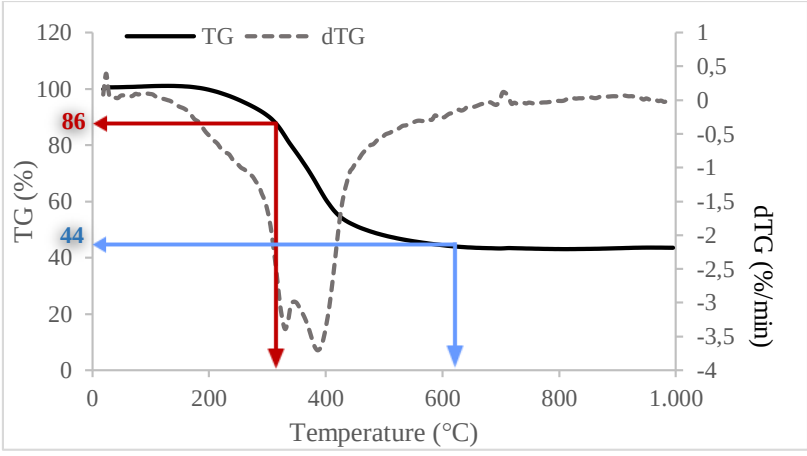

Figure 6. TG and dTG Curves of *PS-P50-250°C-24h*

3.4. The Characteristics of Carbon Foams

3.4.1. Elemental analysis

Elemental analysis results of carbonized foams (*PZCF* and *PZACF*) synthesized from *PS*-based biopitch or after the activation process

were shown in Table 4. Conceiving that the *PS-P50-250°C-24h* biopitch had 73.785% C and 18.695% O contents, the C content of biopitch-based foams after carbonization increased to 91.66% and 84.046%; whereas the O content decreased inversely to 5.736% and 13.570% for *PZCF* and *PZACF*, respectively. In conclusion, higher O and lower C contents were obtained when the activation process was applied after the foaming step compared to the directly synthesized carbon foam.

Table 4. Elemental Analysis Results of Carbon Foams

Foam	**C (%)**	**H (%)**	**O (%)**	**N (%)**
PZCF	91.66	0.71	5.736	1.894
PZACF	84.046	0.552	13.570	1.832

3.4.2. Scanning electron microscope images

Both *PZCF* and *PZACF* had similar cell sequences at 200x magnification of SEM images (Figure 7). Although the pores of the *PZCF* carbon foam were partially closed, the pores of the *PZACF* were relatively open, and also micro-cracks formed in the material structure. It was observed clearly that the formation of windows, which allowed adjacent cells to connect, in the carbon wall developed with the KOH activation. The opening of the pores caused an enhancement in the surface area and thus a reduction in the compressive strength. While there were cells of various sizes in the range of 200-520 μm in the structure of the non-activated foam, it was found out that smaller cells and a more regular pore network were originated in the 40-335 μm range, thus the porosity was increased after the activation process.

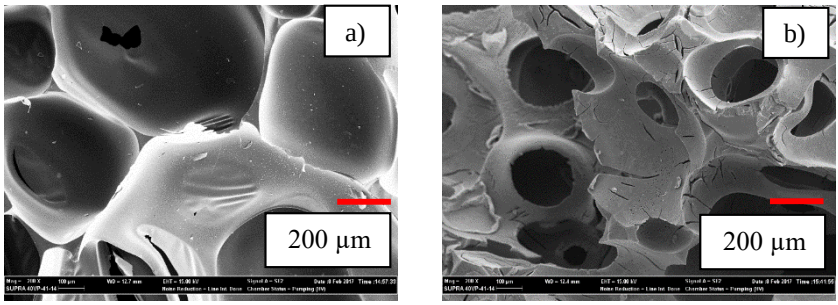

Figure 7. SEM Images of a) *PZCF* and b) P*ZACF*

3.4.3. X-ray diffraction patterns

XRD parameters and diffraction patterns of biopitch-based non-activated and activated carbon foams were offered in Table 5 and Figure 8. In the X-ray diffraction patterns, (1 0 0) and (0 0 2) planes were specified as two characteristic planes particular to carbon-based materials.

The broadband stacked graphitic basal plane (0 0 2), the maximum value of which was around 2θ=23° in XRD patterns of all carbonaceous materials and detected in the range of 2θ=10°–30°, was also identified in diffraction patterns of pistachio shell biopitch-based carbon foams (Apaydın-Varol & Erülken, 2015; Girgis, et al., 2002; Lopez, et al., 2013; Ozbay & Yargic, 2019; Tushar, et al., 2012; Zhang, et al., 2014). Besides, the diffraction peaks around 2θ=23° and 43° corresponded to the planes of hexagonal carbon (0 0 2) and hexagonal graphite (1 0 0), respectively (Gamllen & White, 1976; Hull, 1926; Li, et al., 2014; Lipson and Stokes, 1942; Strano, et al., 2002; Wang, et al., 2012); and the peak around 2θ=72° belonged to orthorhombic graphite (Fayos, 1999). It was proven that the thermoplastic property of the biopitch and small molecules in the structure prepossessed the structural arrangement even at a low carbonization temperature of 1050 °C and promote the development of carbon crystals (Prauchner et al., 2005).

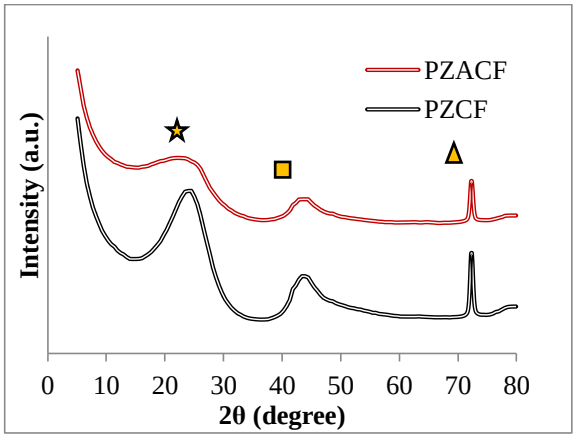

Figure 8. X-Ray Diffraction Patterns of *PZCF* and *PZACF* (★: Hexagonal Carbon, ■ : Hexagonal Graphite, ▲: Orthorhombic Graphite)

Table 5. XRD Parameters of *PZCF* and *PZACF*

Foam	**2θ (002)** (°)	**d_{002}** (nm)	**2θ (100)** (°)	**d_{100}** (nm)
PZCF	23.95	0.3713	43.38	0.2084
PZACF	23.01	0.3862	43.38	0.2084

3.4.4. Structural analysis

Nitrogen sorption isotherms and pore size distributions, which were analyzed to elucidate the pore structures of carbon foams, were shown in Figure 9, and also BET surface area, pore-volume, and average pore

diameter values were given in Table 6. Following the SEM analysis, the surface area value (783,171 m^2/g) of the carbon foam (*PZACF*), which had an open porous structure as a result of chemical activation, was much higher than the surface area (1,334 m^2/g) of the unactivated carbon foam (*PZCF*). The adsorption/desorption isotherms of the carbon foams conformed to the type IV isotherm implying the presence of micro and mesopores according to the IUPAC classification. When the pore size distribution plots were investigated, it was designated that the *PZCF* carbon foam had an average pore diameter of 2.60 nm and showed a regular pore size distribution. It was concluded that the size of the smaller pores formed during the chemical activation process in the structure of the *PZACF* was not uniform, but the average pore diameter (1.22 nm) value shifted towards the micropore range, thus the surface area was improved.

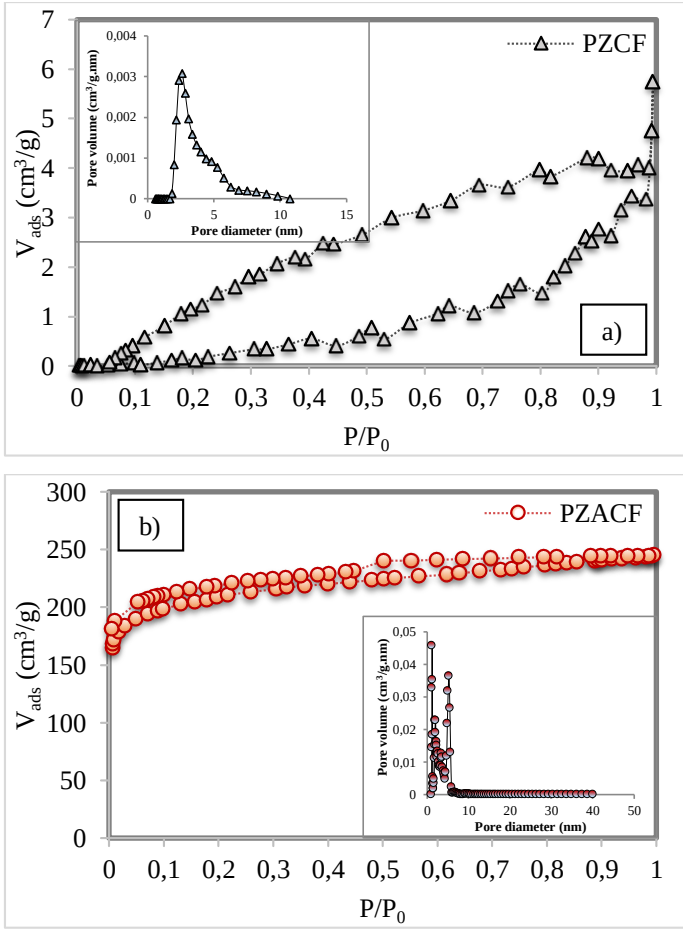

Figure 9. Nitrogen Sorption Isotherms and Pore Size Distribution Plots of a) *PZCF* and b) *PZACF*

Table 6. Structural Properties of Carbon Foams

Foam	S_{BET} (m^2/g)	V_{total} (cm^3/g)	V_{micro} (cm^3/g)	V_{meso} (cm^3/g)	Average pore diameter (nm)
PZCF	1.334	6.1686	0.0002	6.1684	2.60
PZACF	783.171	0.3623	0.3083	0.0540	1.22

3.4.5. Compressive strength and porosity(%)

It is known that the cell structure and density of porous carbon foam are directly related to its strength and thermal conductivity. Increasing the number of micro and mesopores in the foam structure improves porosity but diminishes its strength value (Luo, et al., 2013; Yargic & Ozbay, 2019). The porosity(%) was calculated due to the actual and bulk density values specified in Table 7. Hereunder, depending on the formation of windows connecting adjacent cells by chemical activation process, the porosity value of *PAZCF* carbon foam was calculated as 91.32% while *PACF*'s was 87.96%. However, the compressive strength test results revealed that *PZACF* strength value decreased by 71.36% compared to *PZCA* carbon foam, inversely proportional to porosity(%). The results obtained were in accordance with the scanning electron microscope images and surface area values, and the properties of the material were diversified with the chemical activation process.

Table 7. Compressive Strength and Porosity(%) Values of Biopitch-Based Carbon Foams

Foam	Strength (MPa)	Bulk density (g/cm^3)	Actual density (g/cm^3)	Porosity (%)
PZCF	0.887	0.1902	1.5795	87.96
PZACF	0.254	0.1535	1.7689	91.32

4. Conclusion

In recent years, studies on the selection of sustainable precursors in the production of carbonaceous materials, optimizing the synthesis conditions, and arranging the product properties to suit the application area have come to the fore. In the study, it was aimed to obtain tar from the pistachio shell, which was a household biomass waste, by pyrolysis process at 400 °C, and to evaluate the biopitch produced by vacuum distillation of tar in carbon foam production. In this context, the effects of

the chemical activation process on carbon foam properties were studied in detail. The properties of the carbon foam (CHN content, compressive strength, crystalline structure, morphology, surface area, etc.) were significantly changed due to the formation of interconnected open cells in the biopitch-based foam structure as a result of the chemical activation process. It was determined that the C content of the carbon foam (*PZCF*) synthesized without chemical activation was 9% higher than the *PZACF* foam. Considering the compressive strength values, *PZCF* carbon foam was 3.49 times more resistant than *PZACF* foam. Compared to the *PZCF* foam produced without chemical activation, the porosity of *PZACF* carbon foam was raised by 3.82%, which supported the presence of micropores in the structure and confirmed the enhancement in surface area. As a result, it is possible to synthesize high-tech materials such as carbon foam from nutshells by applying simpler and economical processes as an alternative to the high temperature/pressure conditions required in the processing of coal and petroleum-based pitches and to tailor their properties via process parameters.

References

Antunes, M., & Velasco, J. I. (2014). Multifunctional polymer foams with carbon nanoparticles. *Progress in Polymer Science*, *39*(3), 486-509.

Apaydın-Varol, E., & Erülken, Y. (2015). A study on the porosity development for biomass-based carbonaceous materials. *Journal of the Taiwan Institute of Chemical Engineers*, *54*, 37-44.

Araujo, R. C. S., & Pasa, V. M. D. (2003). Mechanical and thermal properties of polyurethane elastomers based on hydroxyl-terminated polybutadienes and biopitch. *Journal of applied polymer science*, *88*(3), 759-766.

Araújo, R. C. S., & Pasa, V. M. D. (2004). New Eucalyptus tar-derived polyurethane coatings. *Progress in Organic Coatings*, *51*(1), 6-14.

Chithra, A., Wilson, P., Vijayan, S., Rajeev, R., & Prabhakaran, K. (2020). Carbon foams with low thermal conductivity and high EMI shielding effectiveness from sawdust. *Industrial Crops and Products*, *145*, 112076.

Elgafy, A., & Mishra, S. (2014). A heat transfer model for incorporating carbon foam fabrics in firefighter's garment. *Heat and Mass Transfer*, *50*(4), 545-557.

Fayos, J. (1999). Possible 3D carbon structures as progressive intermediates in graphite to diamond phase transition. *Journal of Solid State Chemistry*, *148*(2), 278-285.

Gamlen, P. H., & White, J. W. (1976). Structure and dynamics of microcrystalline graphite, graphon, by neutron scattering. *Journal of the Chemical Society, Faraday Transactions 2: Molecular and Chemical Physics*, *72*, 446-455.

Gao, N., Cheng, B., Hou, H., & Zhang, R. (2018). Mesophase pitch based carbon foams as sound absorbers. *Materials Letters*, *212*, 243-246.

Girgis, B. S., Yunis, S. S., & Soliman, A. M. (2002). Characteristics of activated carbon from peanut hulls in relation to conditions of preparation. *Materials Letters*, *57*(1), 164-172.

Harker, J. H., & Backhurst, J. R. (1981). Fuel and energy. Academic Press Limited, London.

Hull, A. (1926). Berichte der Deutschen Chemischen Gesellschaft. 59, 2433-2444.

Li, W., Huang, Z., Wu, Y., Zhao, X., & Liu, S. (2015). Honeycomb carbon foams with tunable pore structures prepared from liquefied larch sawdust by self-foaming. *Industrial Crops and Products*, *64*, 215-

223. Lipson, H., & Stokes, A. R. (1942). A new structure of carbon. *Nature*, *149*(3777), 328-328.

Liu, H., Li, T., Wang, X., Zhang, W., & Zhao, T. (2014). Preparation and characterization of carbon foams with high mechanical strength using modified coal tar pitches. *Journal of Analytical and Applied Pyrolysis*, *110*, 442-447.

Lopez, F. A., Centeno, T. A., Garcia-Diaz, I., & Alguacil, F. J. (2013). Textural and fuel characteristics of the chars produced by the pyrolysis of waste wood, and the properties of activated carbons prepared from them. *Journal of Analytical and Applied Pyrolysis*, *104*, 551-558.

Luo, X., Mohanty, A., & Misra, M. (2013). Lignin as a reactive reinforcing filler for water-blown rigid biofoam composites from soy oil-based polyurethane. Industrial Crops and Products, 47, 13-19.

Lv, Y., Gan, L., Liu, M., Xiong, W., Xu, Z., Zhu, D., & Wright, D. S. (2012). A self-template synthesis of hierarchical porous carbon foams based on banana peel for supercapacitor electrodes. *Journal of Power Sources*, *209*, 152-157.

Melo, B. N., & Pasa, V. M. (2003). Composites based on eucalyptus tar pitch/castor oil polyurethane and short sisal fibers. *Journal of applied polymer science*, *89*(14), 3797-3802.

Micheli, D., Morles, R. B., Marchetti, M., Moglie, F., & Primiani, V. M. (2014). Broadband electromagnetic characterization of carbon foam to metal contact. *Carbon*, *68*, 149-158.

Ozbay, N., & Yargic, A. S. (2019). Carbon foam production from bio-based polyols of liquefied spruce tree sawdust: Effects of biomass/solvent mass ratio and pyrolytic oil addition. *Journal of Applied Polymer Science*, *136*(11), 47185.

Prauchner, M. J., Pasa, V. M., Molhallem, N. D., Otani, C., Otani, S., & Pardini, L. C. (2005). Structural evolution of Eucalyptus tar pitch-based carbons during carbonization. *Biomass and Bioenergy*, *28*(1), 53-61.

Prauchner, M. J., Pasa, V. M., Otani, C., Otani, S., & de Menezes, S. M. (2004). Eucalyptus tar pitch pretreatment for carbon material processing. *Journal of applied polymer science*, *91*(3), 1604-1611.

Rocha, J. D., Coutinho, A. R., & Luengo, C. A. (2002). Biopitch produced from eucalyptus wood pyrolysis liquids as a renewable binder for carbon electrode manufacture. *Brazilian Journal of Chemical Engineering*, *19*(2), 127-132.

Strano, M. S., Zydney, A. L., Barth, H., Wooler, G., Agarwal, H., & Foley, H. C. (2002). Ultrafiltration membrane synthesis by nanoscale templating of porous carbon. *Journal of membrane science*, *198*(2), 173-186.

Sun, Y., & Webley, P. A. (2011). Preparation of activated carbons with large specific surface areas from biomass corncob and their adsorption equilibrium for methane, carbon dioxide, nitrogen, and hydrogen. *Industrial & engineering chemistry research*, *50*(15), 9286-9294.

Tondi, G., Pizzi, A., Delmotte, L., Parmentier, J., & Gadiou, R. (2010). Chemical activation of tannin–furanic carbon foams. *Industrial Crops and Products*, *31*(2), 327-334.

Tushar, M. S. H. K., Mahinpey, N., Khan, A., Ibrahim, H., Kumar, P., & Idem, R. (2012). Production, characterization and reactivity studies of chars produced by the isothermal pyrolysis of flax straw. *Biomass and bioenergy*, *37*, 97-105.

Tzvetkov, G., Tsyntsarski, B., Balashev, K., & Spassov, T. (2016). Microstructural investigations of carbon foams derived from modified coal-tar pitch. *Micron*, *89*, 34-42.

Velasco, L. F., Tsyntsarski, B., Petrova, B., Budinova, T., Petrov, N., Parra, J. B., & Ania, C. O. (2010). Carbon foams as catalyst supports for phenol photodegradation. *Journal of Hazardous Materials*, *184*(1-3), 843-848.

Wang, R., Li, W., & Liu, S. (2012). A porous carbon foam prepared from liquefied birch sawdust. *Journal of Materials Science*, *47*(4), 1977-1984.

Wang, Y., He, Z., Zhan, L., & Liu, X. (2016). Coal tar pitch based carbon foam for thermal insulating material. *Materials Letters*, *169*, 95-98.

Yaman, E., Yargic, A. S., Ozbay, N., Uzun, B. B., Kalogiannis, K. G., Stefanidis, S. D., Pachatouridou, E. P., Iliopoulou, E. F., & Lappas, A. A. (2018). Catalytic upgrading of pyrolysis vapours: Effect of catalyst support and metal type on phenolic content of bio-oil. *Journal of Cleaner Production*, *185*, 52-61.

Yargıç, A. Ş., Şahin, R. Z. Y., & Özbay, N (2021). Investigation of solvent type effect on the structural properties of bio-polyol-based carbon foam. *Journal of the Faculty of Engineering and Architecture of Gazi University*, *36*(1), 133-146.

Yargic, A. S., & Ozbay, N. (2019). Effect of chemical activation on the cellular structure of biopitch-derived green carbon foam. *Diamond and Related Materials*, *96*, 58-66.

Zhang, S., Zheng, M., Lin, Z., Li, N., Liu, Y., Zhao, B., Pang, H., Cao, J., He, P., & Shi, Y. (2014). Activated carbon with ultrahigh specific surface area synthesized from natural plant material for lithium–sulfur batteries. *Journal of Materials Chemistry A, 2*(38), 15889-15896.